Spatiotemporal simulation of nickel oxide and carbon phases formation in solid oxide fuel cells (SOFC)

J. P. Neidhardt[1,2], V. Yurkiv[1,2], W. G. Bessler[3]

[1]German Aerospace Centre (DLR), Institute of Technical Thermodynamics, 70569 Stuttgart, Germany

[2]Institute of Thermodynamics and Thermal Engineering (ITW), University of Stuttgart, 70550 Stuttgart, Germany

[3]Offenburg University of Applied Sciences, Badstrasse 24, 77652 Offenburg, Germany

jonathan.neidhardt@dlr.de

Keywords: Solid oxide fuel cell (SOFC), degradation, reoxidation, coking, kinetic modeling

ABSTRACT

The formation of secondary phases in the porous electrodes is a severe mechanism affecting the lifetime of solid oxide fuel cells (SOFC). It can occur via various chemical mechanisms and it has a significant influence on cell performance due to pore clogging and deactivation of active surfaces and triple-phase boundary (TPB). We present a modeling and simulation study of nickel oxide formation (reoxidation) and carbon formation (coking) within the SOFC anode.

We use a 2D continuum model based on a multi-phase framework [Neidhardt et al., *J. Electrochem. Soc.*, **159**, 9 (2012)] that allows the introduction of arbitrary solid phases (here: Ni, YSZ, NiO, Carbon) plus gas phase. Reactions between the bulk phases are modeled via interface-adsorbed species and are described by an elementary kinetic approach. Published experimental data are used for parameterization and validation. Simulations allow the prediction of cell performance under critical operation conditions, like (*i*) a non-fuel operation test, where NiO formation is taking place (Figure 1a), or (*ii*) an open circuit voltage (OCV) stability test under hydrocarbon atmosphere, where solid carbon is formed(Figure 1b). Results are applied for enhanced interpretation of experimental data and for prediction of safe operation conditions.

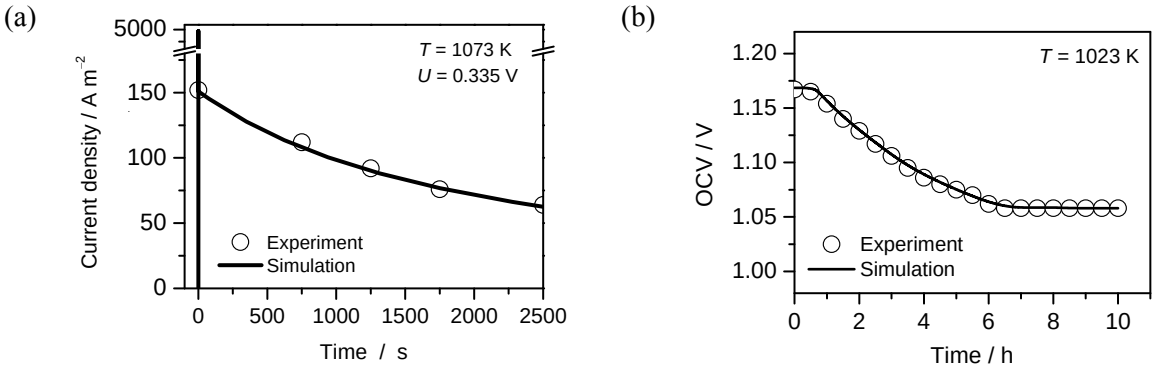

Figure 1. Comparison between experimental and simulated performance of a Ni/YSZ based SOFC anode. (a) Non-fuel operation test at constant voltage of 0.335 V at 1073 K (experimental results taken from Wang et al. [*Electrochem. Commun.*, **11,** 7 (2009)]) and (b) OCV stability test under hydrocarbon atmosphere at 1023 K (experimental results taken from Chen et al. [*J. Power Sources*, **196**, 2461 (2011)]).

1. INTRODUCTION

Solid oxide fuel cells are a promising technology for supplying energy for future demands. SOFC generates electricity by converting chemical energy of reactants directly and continuously into electricity, using fuels like hydrogen ($H_2 + ½\ O_2 \rightleftarrows H_2O$ + energy), syngas ($H_2 + CO + O_2 \rightleftarrows H_2O + CO_2$ + energy) or hydrocarbons ($CH_4 + O_2 \rightleftarrows CO_2 + H_2O$ + energy). This process is highly efficient with more than 50% fuel-to-electricity conversion [1] and even up to 85% for combined heat and power (CHP) [2]. It has been demonstrated that SOFC is well-suited electrical power source for a variety of applications, ranging from mobile technology to stationary power plants. However, the aim for market access is securing a minimum lifetime of 40,000 hours without significant degradation [3]. Therefore, understanding the origin and evolution of degradation processes, which typically take place on micro- and nanoscales, is essential to develop long-term-operating SOFC technology. Two major severe mechanisms affecting the lifetime of SOFC are oxidation of the nickel electrode and solid carbon formation at/in the nickel electrode.

Considering nickel oxide (NiO) formation, the so-called redox behavior and its effects on durability of SOFC are well known from experiments. Main problem is the volume increase of oxidizing nickel particles, due to a change of molar volume by 69.9 % between Ni and NiO [4]. This produces mechanical stresses inside the porous anode structure [5], which can cause anode extension [6,7], cracks [8,9] and delamination from the electrolyte [10]. Additionally, NiO is an insulating material with very low ionic and electronic conductivity [11]. Furthermore, a layer of NiO can block the three-phase boundary (TPB) between nickel, electrolyte and gas-phase causing a break-down of the anodic charge-transfer reaction (CTR). Another effect which has been observed is the reconfiguration of nickel particles during reoxidation cycles, which can permanently decrease the TPB length [12].

Similarly to nickel oxidation, the process of carbon formation at Ni/YSZ based SOFC anodes has been investigated for many years [13,14]. It was identified that the type and amount of formed carbon at Ni/YSZ anode depends upon many factors, e.g. types of fuel, anode morphology, steam to carbon ratio, operating condition etc. This was shown by a pioneering study of Bartholomew [15], who described five major carbon types at Ni such as adsorbed, carbide, polymeric, graphitic, vermicular and filaments. Generally, under typical SOFC working conditions, all of these carbon types could be classified into two major formation mechanisms: (*i*) heterogeneously formed carbon that grows on nickel catalytic surface primary as a film, blocking heterogeneous and electrochemistry, and (*ii*) homogeneously/heterogeneously formed soot (pyrolytic carbon), which blocks pores increasing mass transfer resistance [16].

The model developed in this work represents coupled processes of chemistry, transport and degradation mechanisms at the Ni/YSZ based SOFC anode. The present approach incorporates elementary heterogeneous chemical reactions, electrochemical charge-transfer, multicomponent porous-phase and channel-phase transport, and electrode degradation due to nickel oxidation and carbon formation. The simulation results are used to analyze available literature experimental data of anode-supported SOFC.

2. MODELING AND SIMULATION METHODOLOGY

We use a 2D model of a planar SOFC. The model includes coupled electrochemistry and transport through membrane-electrode assembly (MEA) and gas channels. Anode electrochemistry is described using elementary kinetics for surface reactions on Ni and YSZ, and for charge transfer [17]. Cathode electrochemistry is described using a modified Butler-Volmer equation introduced by Zhu an co-workers [18]. Current-voltage relationships are modeled by directly solving for the electric-potential distribution in the electrodes and electrolyte without using the Nernst equation. The evolution of nickel oxide and carbon inside the anode are quantified by a multi-phase modeling approach [19]. The latter is accounting for the volume fractions (ε) of all phases as a function of time and spatial location inside the cell, by taking into account the chemical rate laws of all involved reactions and overall mass conservation.

Formation of nickel oxide and carbon phase inside the Ni/YSZ anode is schematically depicted in Figure 2. NiO is formed in case of high steam content or low cell voltages. A film of carbon can be formed during operation with hydrocarbons. Both secondary phases can reduce the Ni surface area as well as the TPB length, thus decreasing the cell performance.

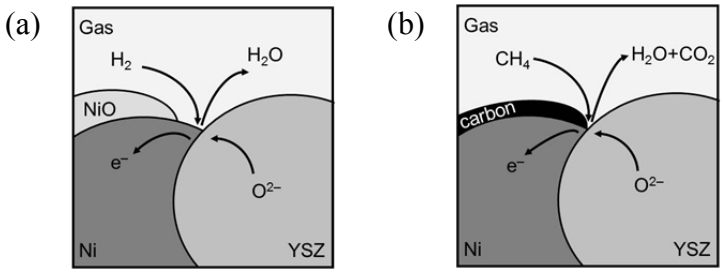

Figure 2. Illustration of NiO (a) and carbon (b) formation at Ni/YSZ SOFC anode.

2.1 Model for NiO formation

Oxidation of the nickel phase can take place via two different pathways, thermochemical and electrochemical oxidation [20]. Thermochemical oxidation is implemented in the model as elementary-kinetic reaction of bulk nickel with oxygen attached to the Ni surface. Thus oxidation by air and by water vapor can be covered by one reversible reaction,

$$Ni_{Ni}^{X} + O_{Ni} \rightleftarrows NiO + \square_{Ni}, \quad (5)$$

where, Ni_{Ni}^{X} is bulk lattice nickel atom, O_{Ni} is a surface-adsorbed oxygen atom and $\square_{Ni}$ is a free nickel surface site. Electrochemical oxidation is described by a global reaction at the interface between the nickel and YSZ bulk phases,

$$Ni_{Ni}^{X} + O_{O\,YSZ}^{X} \rightleftarrows NiO + V_{YSZ}^{\cdot\cdot} + 2\,e^{-}, \quad (6)$$

where, $O_{O\,YSZ}^{X}$ indicates doubly negative charged YSZ bulk oxygen and $V_{YSZ}^{\cdot\cdot}$ is an oxygen vacancy.

The size of all interfaces in-between bulk phases can be scaled to model microstructural changes during bulk-phase deposition. This includes, e.g., modeling phase formation processes, or the feedback of nickel oxide on the length of the electrochemical active TPB of the anode ($l^{\mathrm{V}}_{\text{Ni-YSZ-Gas}}$). For the latter we use an empirical exponential function; at a degree of oxidation (DOO) of 1% the TPB is reduced by a factor of 10,

$$l^{\mathrm{V}}_{\text{Ni-YSZ-Gas}} = l^{\mathrm{V}}_{\text{Ni-YSZ-Gas,0}} \cdot \exp\left(-2.3 \cdot \mathrm{DOO}\right), \tag{7}$$

where, a subscript $_0$ denotes the initial TPB length. The DOO is defined as proportion of nickel oxide in the total volume filled by Ni and NiO,

$$\mathrm{DOO} = \frac{\varepsilon_{\mathrm{NiO}}}{\varepsilon_{\mathrm{Ni}} + \varepsilon_{\mathrm{NiO}}} \quad . \tag{8}$$

A second feedback mechanism of secondary phase formation on cell performance is implemented by anode porosity reduction. This directly affects the effective diffusivity of gas-phase species which is described by

$$D_i^{\mathrm{eff}} = \frac{\varepsilon_{\mathrm{Gas}}}{\tau^2_{\mathrm{Gas}}} D_i \quad , \tag{9}$$

where, D_i describes the diffusion coefficient of species i and τ the tortuosity of the gas-phase.

A scaling function is used to represent the initial process of phase formation. The surface of a not-existing phase is zero. In order to avoid numerical instabilities, which may occur when reaching volume fractions equal to zero, we assume that the boundary to adjacent phases vanishes for very low volume fractions, according to

$$A^V = A_0^V \cdot \tanh(10^9 \varepsilon) \quad , \tag{10}$$

where A_0^{V} is the initial surface area.

2.2 Model for carbon formation

Carbon species can be formed on the surface of nickel via different pathways such as hydrocarbon cracking,

$$\mathrm{C}_x\mathrm{H}_y + (x+y)\square_{\mathrm{Ni}} \rightleftarrows x\mathrm{C}_{\mathrm{Ni}} + y\mathrm{H}_{\mathrm{Ni}} \ , \tag{11}$$

hydrocarbon oxidation,

$$\mathrm{C}_x\mathrm{H}_y + (x+y)\mathrm{O}_{\mathrm{Ni}} \rightleftarrows x\mathrm{C}_{\mathrm{Ni}} + y\mathrm{OH}_{\mathrm{Ni}} \ , \tag{12}$$

and Boudouard reaction,

$$x\mathrm{CO} + x\square_{\mathrm{Ni}} \rightleftarrows x/2\mathrm{C}_{\mathrm{Ni}} + x/2\mathrm{CO}_{2,\mathrm{Ni}}\,, \tag{13}$$

The formation of solid carbon as new phase on top of the Ni surface is modeled by an elementary-kinetic reaction of ordinary surface-adsorbed carbon species on the Ni surface (C_{Ni}) from reactions (11)-(13) via following equation:

$$\mathrm{C}_{\mathrm{Ni}} \rightleftarrows \mathrm{C}_{\mathrm{C}}^{\mathrm{X}} + \square_{\mathrm{Ni}}, \tag{14}$$

where, $\mathrm{C}_{\mathrm{C}}^{\mathrm{X}}$ is bulk carbon, which belongs to a newly formed phase on top of the Ni surface.

As it was described above, phase formation is characterized by mass transfer from one phase to another by (electro)-chemical reactions. In the case of carbon phase formation on Ni surface, singly adsorbed carbon species is transferred to a new bulk phase (see Eq. 14). The newly formed carbon phase reduces Ni active surface area and TPB length. In order to describe Ni active area reduction as the function of carbon phase growth, we use a simple linear function as follows

$$A_{\mathrm{Ni}}^{\mathrm{V}} = A_{\mathrm{Ni},0}^{\mathrm{V}} \cdot (1 - \varepsilon_{\mathrm{Carbon}} / \varepsilon_{\mathrm{Carbon}}^{\max})\,, \tag{15}$$

where, $A_{\mathrm{Ni}}^{\mathrm{V}}$ describes volume specific surface area, $A_{\mathrm{Ni},0}^{\mathrm{V}}$ denotes initial volume specific surface area, $\varepsilon_{\mathrm{Carbon}}$ - volume fraction of carbon phase, and $\varepsilon_{\mathrm{Carbon}}^{\max}$ is the maximum possible volume fraction of carbon phase. In the present study we use value of 0.02 for the latter parameter. Detailed explanation of that value is given further below. Since the growth of carbon phase on Ni surface is continuously progressive, it can be assumed that anode TPB is also covered by carbon via a linear relationship similar to Eq. 15,

$$l_{\mathrm{Ni}}^{\mathrm{V}} = l_{\mathrm{Ni},0}^{\mathrm{V}} \cdot (1 - \varepsilon_{\mathrm{Carbon}} / \varepsilon_{\mathrm{Carbon}}^{\max})\,. \tag{16}$$

Here, instead of surface specific area we use TPB length ($l_{\mathrm{Ni}}^{\mathrm{V}}$). Both, Eqs. 15 and 16 reveal that the two geometrical parameters approach zero when volume fraction of carbon reaches its maximum value.

Geometrically, the newly formed carbon phase is characterized by volume fraction, density, TPB length between carbon, Ni and gas-phase, etc. In particular, we assume that carbon formation takes place at the TPB between solid carbon, solid nickel, and the gas phase. It is reasonable to assume that the TPB changes in time while carbon phase is growing. In the present model we assume that the TPB increases at first, reaching appropriate maximum length, and then it decreases to zero, since, there is no more Ni surface available for carbon phase growth. This phenomenon can be described by the following function

$$l_{\mathrm{Carbon}}^{\mathrm{V}} = l_{\mathrm{Carbon},0}^{\mathrm{V}} \cdot \varepsilon_{\mathrm{Carbon}} \cdot (1 - \varepsilon_{\mathrm{Carbon}} / \varepsilon_{\mathrm{Carbon}}^{\max})\,, \tag{17}$$

where, $l_{\mathrm{Carbon}}^{\mathrm{V}}$ is the TPB length of carbon phase, correspondingly, a subscript $_0$ denotes the initial TPB length. It should be also mentioned that the increase of carbon volume fraction directly affects the anode volume fraction and, correspondingly, gas phase species diffusion. Yet again Eq. 9 is used to model the effect of carbon volume fraction on diffusivity.

2.3 Simulation procedure

Simulations were carried out using the in-house software package DENIS (detailed electrochemistry and numerical impedance simulation) [21]. In order to evaluate the chemical source terms, we use the software CANTERA developed by Goodwin and co-workers [22]. We coupled CANTERA to our software DENIS, making the full CANTERA functionality available during DENIS runtime. The computational domain is spatially discretized using the finite-volume method. All model equations are given in detail in Ref. [21]. Experimental electrochemical impedance spectra were simulated using a potential step and current relaxation technique [23]. The impedance is obtained in the frequency domain by a Fourier transformation of the resulting time-domain traces of current and potential. The differential-algebraic equation (DAE) system solver LIMEX [24] is used for the numerical integration of the reaction-diffusion equations.

3. RESULTS

3.1 Nickel oxide phase formation

Determination of thermodynamic and kinetic data
The model has to be parameterized with kinetic data for the thermochemical as well as for the electrochemical oxidation pathway (Eqs. 5 and 6). We use experiments by Hagen et al. [25] and Wang et al. [26] for determination of the preexponential factor for the NiO formation reaction (Eqs. 5 and 6). As activation energy a value of 144±15 kJ mol^{-1} is used [4].

Hagen et al. [25] made a zero-current experiment with two consecutive reduction–oxidation cycles in a SOFC. This experiment is suitable to parameterize the thermochemical parameters because electrochemical oxidation can be excluded when no current load is applied. The temperature was set to 1153 K during the oxidation steps and to 1119 K and 1133 K during the first and second reduction step. The oxidation steps were performed in a flow of 5 $L \cdot h^{-1}$ air and the reductions in helium containing 4% hydrogen at 4 $L \cdot h^{-1}$. Measured data points and simulation curves for thermochemical oxidation and reduction are shown in Figure 3. The preexponential factor was determined to be $2.7 \cdot 10^3$ $m^4 \cdot kmol^{-1} \cdot s^{-1}$.

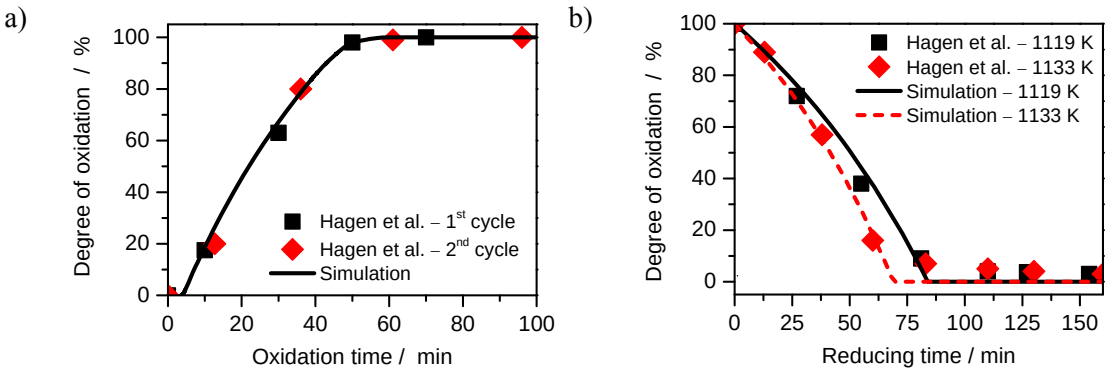

Figure 3. a) Simulated oxidation dynamics of bulk nickel in air at 1153 K compared to experimental data of Hagen et al. [25] . Model kinetic parameters (forward reaction) are fitted to match the experiment. b) Reduction dynamics of bulk nickel oxide in Helium containing

4% H_2 at 1119 K (first cycle) and 1133 K (second cycle) [25]. Model kinetic parameters follow from thermodynamic consistency.

Simulated data for oxidation was shifted by 3.4 minutes because the initially lower reaction kinetics as measured by Hagen (s-shaped curve) could not be reproduced by the present model. Deviations between measured and simulated reduction kinetics can be explained by slithtly inaccuarcies in the thermodynamic data.

The kinetics of electrochemical oxidation can be obtained by a non-fuel current experiment. During potentiostatic operation the hydrogen fuel flow is shot off and replaced with pure nitrogen. Thus the hydrogen oxidation reaction cannot take place anymore and no electricity will be generated on the conventional way. Therefore we can be sure that the whole measured current is produced by the electrochemical nickel oxidation reaction (Eq. 6). The experiment of Wang et al. [26] was performed at 1073 K by holding a fixed voltage of 0.335 V. Measured data points and the best fitted simulation curve for electrochemical oxidation are shown in Figure 1a. The preexponential factor was determined to be $4 \cdot 10^{-7}$ $m^4 \cdot kmol^{-1} \cdot s^{-1}$. To reproduce the slope from the experiment the model had to be enhanced by an additional function which describes the interdependancy between amount of NiO volume fraction and the active surface area between nickel and YSZ ($A^{V}_{\text{Ni-NiO-YSZ}}$). Good agreement could be obtained by applying an exponential decreasing function,

$$A^{V}_{\text{Ni-NiO-YSZ}} = A^{V}_{\text{Ni-NiO-YSZ,0}} \cdot \exp(-50 \cdot \varepsilon_{\text{NiO}}) \tag{18}$$

.

Thermodynamics is implemented as temperature dependent data in form of NASA polynomials [27]. Data for bulk nickel oxide was taken and recalculated from [28].

Simulation results and discussion.

Simulations can be used to analyse the evolution of nickel oxide volume fraction with spatiotemporal resolution. Figure 4 shows the formation of NiO inside the porous Ni/YSZ anode during the oxidation in air at a temperature of 1153 K (cf. Figure 3a). Four time points are chosen, which correspond to the beginning (t = 1 min), the intermediate region (t = 15 min and t = 30 min), and the end (t = 45 min) of the oxidation process. As obvious, NiO formation starts at the gas inlet. Here the highest DOOs are obtained. Parts of the electrode close to the electrolyte layer are less oxidized. After 1 min about half of the anode shows a degree of oxidation > 1%. This indicates that a large part of the nickel phase is already covered by a thin layer of NiO. Nevertheless, the electrochemically active area, which is located in the first 50 to 100 µm from the electrolyte, is not yet affected. Thus, no permanent damage should appear after this exposure time. After 15 min the picture has changed dramatically. Throughout the electrode a minimum DOO of 39% is reached. With this amount of NiO present, the active triple-phase boundary is largely blocked and no more hydrogen reduction is be possible. With a DOO up to 45% close to the channel the probability of permanent cell damage is high. After 30 min the DOO throughout the anode has risen linearly. The degree of oxidation amounts between 70 and 80%. After 45 min the nearly the whole nickel phase is oxidized. Close to the electrolyte the DOO has grown less, due to slow transport through the very small remaining pore space.

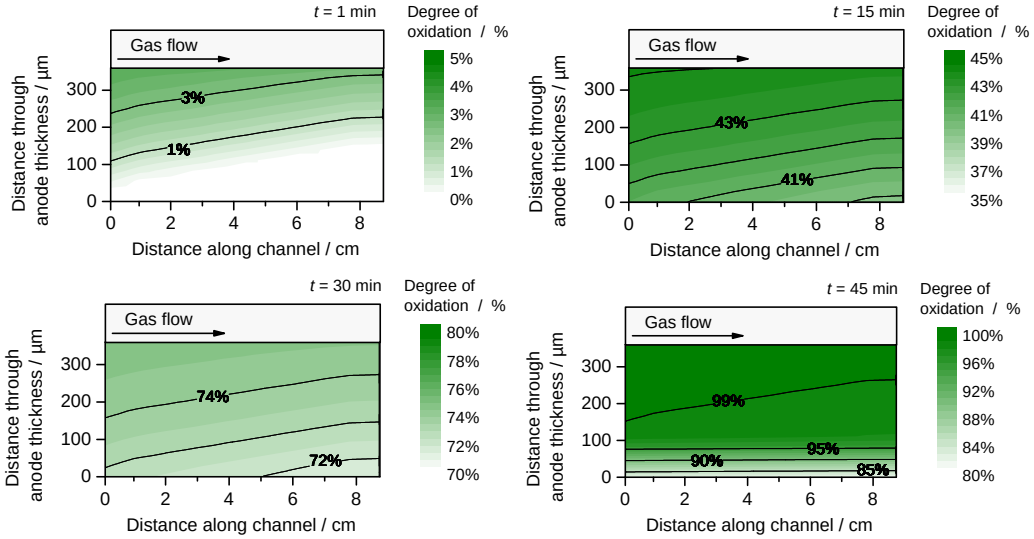

Figure 4. Spatial evolution of degree of oxidation inside the porous anode for four different times corresponding to the simulation shown in Figure 3**Fehler! Verweisquelle konnte nicht gefunden werden.**a.

Spatiotemporal simulations can be applied to identify ‘safe’ and ‘unsafe’ operation parameters. Figure 5 shows a map of conditions for NiO formation according to the global parameters cell voltage and fuel utilization. Each data point shows steady-state operation conditions. Black dots indicate that no nickel oxide is formed inside the electrode, while a DOO > 10^{-4} is represented by a red triangle. Straight lines indicate the local limits of NiO formation as predicted by thermodynamics.

Results show that cell operation far below the limiting voltage of 0.704 V is possible without reoxidation as long as the fuel utilization is low. NiO formation only takes place for a FU > 95%. At high cell voltages cell operation up to the thermodynamically predicted limit of FU = 99.374% is possible.

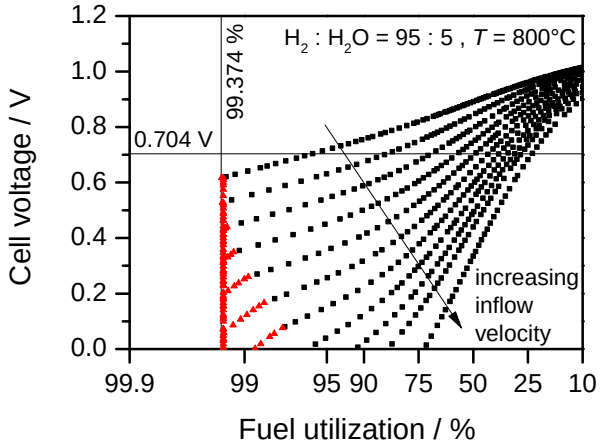

Figure 5. Limiting conditions for nickel oxide formation shown in a set of polarization curves. Red triangles indicate a reoxidation of the anode.

3.2 Carbon phase formation

Heterogeneous chemical mechanism of CH_4 reforming on Ni surface
Since the gas phase assumed in the present work consists of methane and syngas, we use the full mechanism of methane reforming on a nickel surface developed previously by Deutschmann and co-workers [30]. The reaction mechanism consists of 42 surface reactions between 7 gas-phase species and 14 surface-adsorbed species. This mechanism was developed to describe steam reforming (SR), partial oxidation (POX) and dry reforming (DR) of methane. All kinetic and thermodynamic data are taken from Ref. [30].

Kinetic and thermodynamic data of solid carbon phase
As it was described in section 2 (Eq. 14), carbon phase on Ni surface is formed by agglomeration of surface-adsorbed carbon species to the bulk phase. Hence, it is essential to derive thermodynamic data of deposited carbon in the bulk phase. There are a number of studies of thermodynamic properties of carbon in SOFCs [31–33], however, all of them are based upon an assumption that thermodynamic properties of graphite alone can represent the different types of carbon formed at Ni/YSZ anode. Electrochemical and chemical experimental results contradict this assumption, suggesting that thermodynamic properties of carbon, belonging to the newly formed phase on Ni surface, must be determined separately. Efforts to determine thermodynamic properties of deposited carbon were made by Hill and co-workers [34,35], and recently by Lee et al. [19].

Following these works we have derived thermodynamic data (enthalpy and entropy) and kinetics of carbon deposited on the new phase on Ni surface described by Eq. 14. With the intention to derive these data, we used temperature programmed oxidation (TPO) measurements by Alzate-Restrepo et al. [34]. Alzate-Restrepo et al. have performed in-situ investigation of carbon formation at Ni/YSZ anode under typical SOFC operation conditions, including the effect of current density, time and anode thickness. Using our model we have performed TPO simulations in order to determine thermodynamic and kinetic data of bulk carbon on the Ni surface. Figure 6 shows the results of CH_4 TPO measurements taken from Ref. [34], which were obtained at 1073 K and exposure of 6 h (open symbols) along with the results of the present numerical simulations (solid line). For the simulation of carbon formation via Eq. 14, the pre-exponential factor of $5.5 \cdot 10^{16}$ $cm^2 \cdot mol^{-1} \cdot s^{-1}$ along with an activation energy of 30 $kJ \cdot mol^{-1}$ were used. For quantitative reproducibility of TPO spectra, a carbon enthalpy and entropy of –91.2 $kJ \cdot mol^{-1}$ and 32 $J \cdot K^{-1} \cdot mol^{-1}$, respectively, were obtained by fitting.

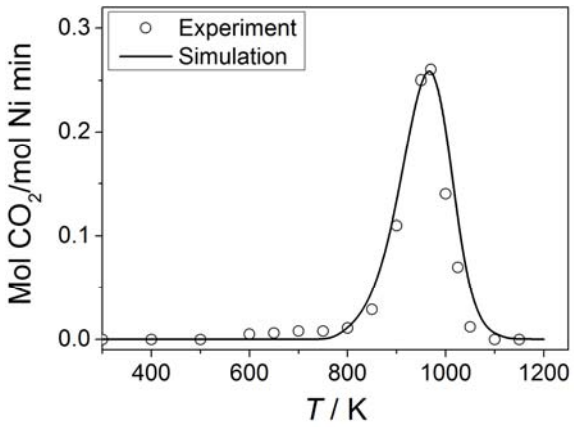

Figure 6. Comparison between experimental and simulated TPO spectra of a Ni/YSZ anode exposed to CH_4 for 6 h at 1073 K at open circuit voltage. Heating rate is 10 $K \cdot min^{-1}$.

Electrochemical simulation results and discussion.

Present electrochemical simulations of carbon formation are used to analyze recent experiments of Chen et al., which were conducted using well-defined and thoroughly-characterized Ni/YSZ based anode-supported SOFC [3]. These experiments stand for the most complete data set available at the present and they cover an extended range of operating temperatures (923 K $\leq T \leq$ 1023 K) and various syngas compositions (see Ref. [3] for detail). In the present work we use the following gas phase composition 23.64 % CH_4, 7.6 % CO, 14.27 % CO_2, 49.48 % H_2, 5 % H_2O (gas composition no. 7 in Ref. [3]) for all simulations. The experimental setup and methodology have been described in detail in Ref. [3] in the above mentioned paper, and only shortly outlined here. In the experiments, Ni/YSZ cermet anodes with substrate thickness of 500 μm and an active area of 4 × 4 cm^2 were used, which were coupled with 8.5 mol-% polycrystalline Y_2O_3–stabilized ZrO_2. The anode support consists of 10 μm thick anode and a 10 μm thick YSZ electrolyte, which were sprayed onto the support substrate followed by sintering at 1623 K for 3h. As for the cathode, 10 μm thick LSM ($La_{0.75}Sr_{0.25}MnO_3$) and 50 wt% YSZ were used. Electrochemical impedance spectra were recorded for different gas phase mixtures at open circuit over a frequency range of 0.1 Hz to 100 kHz with a voltage stimulus of 10 mV.

Fig. 7 shows a comparison between experimental impedance spectra from Ref. [3] (dots) and simulations at T = 1023 K. As described in [3], impedance spectra were recorded at 15, 30 and 45 minutes after gas exposure, similarly to the OCV stability test shown in Fig. 1b. Our model was not able to reproduce these results for this time scale. Instead, we could achieve good agreement by choosing longer exposure times of 50, 70 and 90 minutes. Nevertheless, when looking at the OCV stability test shown in Fig. 1b (both experimental and simulated results), we do not observe significant changes during a period of the first 45 minutes which could cause such a large change of impedance. It was only possible to observe a qualitative agreement between model and experiment over the complete investigated range of experimental conditions using different time ranges.

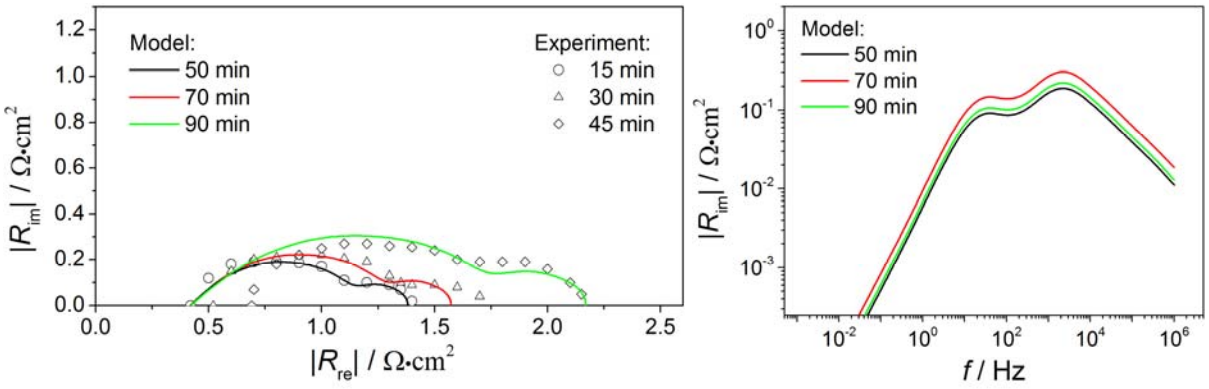

Figure 7. Nyquist (left) and Bode (right) plots of simulated impedance spectra at temperature of 1023 K and pressure 1 atm. The experimental results are taken from [3].

For further insight into the mechanistic details of carbon formation, simulated Ni surface area and Ni TPB length are shown in Fig. 8 as a function of time. These results clearly indicate that newly formed carbon phase covers Ni area as well as Ni TPB blocking heterogeneous and charge-transfer reactions.

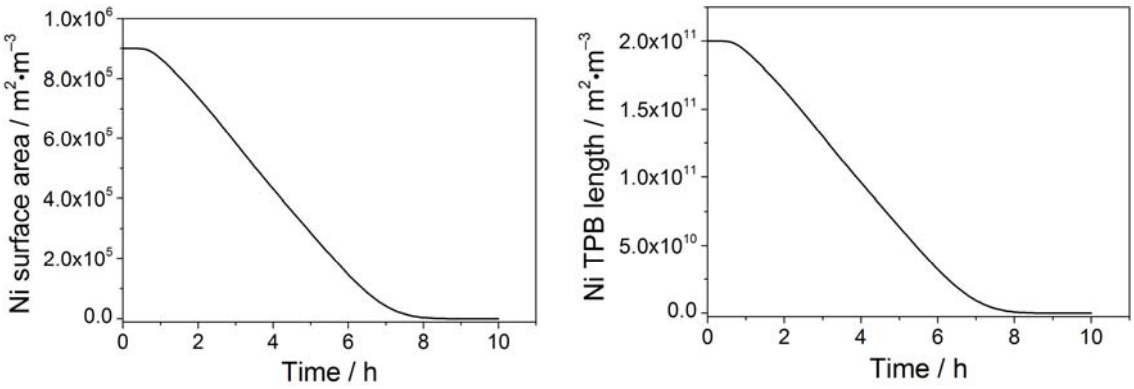

Figure 8. Change of Ni surface specific area and Ni TPB length in time. Ni surface is blocked by solid carbon

When the Ni surface is completely covered, carbon volume fraction is reaching its maximum value (Figure 9). The maximum possible volume fraction of carbon is set as model parameter to 0.02. From thermodynamic point of view the amount of deposited carbon can be theoretically determined considering given experimental conditions. For this reason the maximum possible volume fraction of carbon was chosen based upon thermodynamic calculations using experimental conditions by free energy minimization method [3]. Assuming initial gas phase composition of 100 kmol, temperature 1023 K and 1 atm, thermodynamic calculation of maximum volume fraction of carbon reveals the value of 0.02, which is used as already mentioned in the present model.

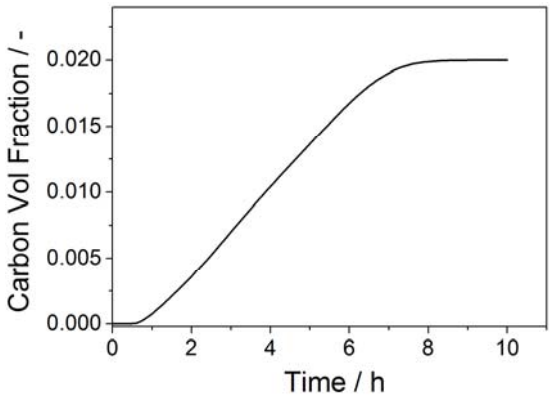

Figure 9. Evolution of carbon volume fraction on Ni surface in time

4. SUMMARY AND CONCLUSIONS

We have presented a combined modeling and experimental study considering different degradation phenomena at Ni/YSZ SOFC anodes. By solving reaction-diffusion equations and phase formation chemistry, different experimental data were successfully reproduced over a wide range of operating conditions. The elementary kinetic description is used throughout the paper, which opens up the possibility of a direct mechanistic interpretation of the experimentally-observed electrochemical characteristics.

Results for nickel reoxidation under hot air atmosphere (1153 K) show that after an exposure time of 1 min, the degree of oxidation is uncritical for cell operation. Nevertheless, after 15 min a huge amount of NiO has formed, blocking the TPB and causing a high probability for mechanical cell failure. Furthermore, simulations allow the prediction of global conditions for

‘safe’ cell operation. A map of safe operation points according to the global parameters cell voltage and fuel utilization shows, that for low fuel utilization even under very low voltages no NiO is formed. In the case of solid carbon formation, the simulation results show that the cell degradation is influenced significantly by the operation temperature and gas phase composition. At OCV and high temperature (1023 K), a surface carbon layer is formed which covers Ni surface and Ni three-phase boundary, blocking heterogeneous and charge-transfer reactions.

The level of understanding achieved in the present study will be the basis for further investigations of the degradation behavior of Ni/YSZ based SOFC anodes.

REFERENCES

[1] S. Curtin, J. Gangi, E. Delmont, F. Cells, The Business Case for Fuel Cells: Why Top Companies are Purchasing Fuel Cells Today, Washington, D.C., 2010.

[2] M. Suzuki, S. Iwata, K. Higaki, S. Inoue, T. Shigehisa, I. Miyachi, et al., Development and Field Test Results of Residential SOFC CHP System, ECS Transactions. 25 (2009) 143-147.

[3] P. Holtappels, R. Steinberger-Wilckens, Realising Reliable, Durable, Energy Efficient and Cost Effective SOFC Systems (Real-SOFC), Fuel Cells. 9 (2009) 783-784.

[4] D. Sarantaridis, A. Atkinson, Redox Cycling of Ni Based Solid Oxide Fuel Cell Anodes: A Review, Fuel Cells. 7 (2007) 246-258.

[5] T. Klemenso, C. Chung, P.H. Larsen, M. Mogensen, The mechanism behind redox instability of anodes in high-temperature SOFCs, Journal of the Electrochemical Society. 152 (2005) A2186-A2192.

[6] A. Faes, A. Hessler-Wyser, D. Presvytes, C.G. Vayenas, J. Van Herle, Nickel-Zirconia Anode Degradation and Triple Phase Boundary Quantification from Microstructural Analysis, Fuel Cells. 9 (2009) 841-851.

[7] M. Pihlatie, A. Kaiser, M. Mogensen, Redox stability of SOFC: Thermal analysis of Ni-YSZ composites, Solid State Ionics. 180 (2009) 1100-1112.

[8] M. Ettler, H. Timmermann, J. Malzbender, A. Weber, N.H. Menzler, Durability of Ni anodes during reoxidation cycles, Journal of Power Sources. 195 (2010) 5452-5467.

[9] D. Sarantaridis, R.A. Rudkin, A. Atkinson, Oxidation failure modes of anode-supported solid oxide fuel cells, Journal of Power Sources. 180 (2008) 704-710.

[10] J. Laurencin, G. Delette, B. Morel, F. Lefebvre-Joud, M. Dupeux, Solid Oxide Fuel Cells damage mechanisms due to Ni-YSZ re-oxidation: Case of the Anode Supported Cell, Journal of Power Sources. 192 (2009) 344-352.

[11] J. Yu, K.M. Rosso, S.M. Bruemmer, Charge and Ion Transport in NiO and Aspects of Ni Oxidation from First Principles, The Journal of Physical Chemistry C. 116 (2012) 1948-1954.

[12] T. Matsui, R. Kishida, J.-Y. Kim, H. Muroyama, K. Eguchi, Performance Deterioration of Ni–YSZ Anode Induced by Electrochemically Generated Steam in Solid Oxide Fuel Cells, Journal of The Electrochemical Society. 157 (2010) B776.

[13] S. McIntosh, R.J. Gorte, Direct hydrocarbon solid oxide fuel cells., Chemical Reviews. 104 (2004) 4845-65.

[14] D. Mogensen, J.-D. Grunwaldt, P.V. Hendriksen, K. Dam-Johansen, J.U. Nielsen, Internal steam reforming in solid oxide fuel cells: Status and opportunities of kinetic studies and their impact on modelling, Journal of Power Sources. 196 (2011) 25-38.

[15] C.H. Bartholomew, Catalysis Reviews : Science and Reforming and Methanation Carbon Deposition in Steam Reforming and Methanation, Cat. Rev.-Sci. Eng. 24 (1982) 67-112.

[16] W.Y. Lee, J. Hanna, a. F. Ghoniem, On the Predictions of Carbon Deposition on the Nickel Anode of a SOFC and Its Impact on Open-Circuit Conditions, J. Electrochem. Soc. 160 (2012) F94-F105.

[17] M. Vogler, A. Bieberle-Hutter, L. Gauckler, J. Warnatz, W.G. Bessler, Modelling Study of Surface Reactions, Diffusion, and Spillover at a Ni/YSZ Patterned Anode, Journal of the Electrochemical Society. 156 (2009) B663-B672.

[18] H. Zhu, R.J. Kee, V.M. Janardhanan, O. Deutschmann, D.G. Goodwin, Modeling elementary heterogeneous chemistry and electrochemistry in solid-oxide fuel cells, Journal of the Electrochemical Society. 152 (2005) A2427.

[19] J.P. Neidhardt, D.N. Fronczek, T. Jahnke, T. Danner, B. Horstmann, W.G. Bessler, A Flexible Framework for Modeling Multiple Solid, Liquid and Gaseous Phases in Batteries and Fuel Cells, Journal of the Electrochemical Society. 159 (2012) A1528-A1542.

[20] J. Neidhardt, M. Henke, W.G. Bessler, Kinetic Modeling of Nickel Oxidation in SOFC Anodes, ECS Transactions. 35 (2011) 1621-1629.

[21] W.G. Bessler, S. Gewies, M. Vogler, A new framework for physically based modeling of solid oxide fuel cells, Electrochimica Acta. 53 (2007) 1782-1800.

[22] D.G. Goodwin, Cantera, in: Http://code.google.com/p/cantera/, 2001-2012, n.d.

[23] W.G. Bessler, A new computational approach for SOFC impedance from detailed electrochemical reaction–diffusion models, Solid State Ionics. 176 (2005) 997-1011.

[24] P. Deuflhard, E. Hairer, J. Zugck, One-Step and Extrapolation Methods for Differential-Algebraic Systems, Numerische Mathematik. 51 (1987) 501-516.

[25] A. Hagen, H.F. Poulsen, T. Klemenso, R.V. Martins, V. Honkimaeki, T. Buslaps, et al., A depth-resolved in-situ study of the reduction and oxidation of Ni-based anodes in solid oxide fuel cells, Fuel Cells. 6 (2006) 361-366.

[26] C.-H. Wang, M.-C. Lee, T.-J. Huang, Y.-C. Chang, W.-X. Kao, T.-N. Lin, Breeding phenomenon of nickel in anode of solid oxide fuel cell via electrochemical reaction, Electrochemistry Communications. 11 (2009) 1381-1384.

[27] B.J. McBride, M.J. Zehe, S. Gordon, NASA Glenn coefficients for calculating thermodynamic properties of individual species, National Aeronautics and Space Administration, John H. Glenn Research Center at Lewis Field, 2002.

[28] R.D. Holmes, H.S.C. O'Neill, R.J. Arculus, Standard Gibbs free energy of formation for Cu2O, NiO, CoO, and FexO: High resolution electrochemical measurements using zirconia solid electrolytes from 900-1400 K, Geochimica Et Cosmochimica Acta. 50 (1986) 2439-2452.

[29] L. Maier, B. Schädel, K. Herrera Delgado, S. Tischer, O. Deutschmann, Steam Reforming of Methane Over Nickel: Development of a Multi-Step Surface Reaction Mechanism, Topics in Catalysis. 54 (2011) 845-858.

[30] J.-H. Koh, B.-S. Kang, H.C. Lim, Y.-S. Yoo, Thermodynamic Analysis of Carbon Deposition and Electrochemical Oxidation of Methane for SOFC Anodes, Electrochemical and Solid-State Letters. 4 (2001) A12.

[31] J. Liu, S.A. Barnett, Operation of anode-supported solid oxide fuel cells on methane and natural gas, Solid State Ionics. 158 (2003) 11-16.

[32] K. Sasaki, Y. Teraoka, Equilibria in Fuel Cell Gases, J. Electrochem. Soc. 150 (2003) A885.

[33] V. Alzate-Restrepo, J.M. Hill, Effect of anodic polarization on carbon deposition on Ni/YSZ anodes exposed to methane, Appl. Cat. A: General. 342 (2008) 49-55.

[34] V. Alzate-Restrepo, J.M. Hill, Carbon deposition on Ni/YSZ anodes exposed to CO/H2 feeds, J. Power Sources. 195 (2010) 1344-1351.

[35] T. Chen, W.G. Wang, H. Miao, T. Li, C. Xu, Evaluation of carbon deposition behavior on the nickel/yttrium-stabilized zirconia anode-supported fuel cell fueled with simulated syngas, J. Power Sources. 196 (2011) 2461-2468.